Orientation and energy dependence of NO scattering from Pt(111)

R. J. W. E. Lahaye
FOM-Institute for Atomic and Molecular Physics, Kruislaan 407, 1098 SJ Amsterdam, The Netherlands and Physical Chemistry and Laser Centre, Vrije Universiteit, De Boelelaan 1083, 1081 HV Amsterdam, The Netherlands

S. Stolte
Physical Chemistry and Laser Centre, Vrije Universiteit, De Boelelaan 1083, 1081 HV Amsterdam, The Netherlands

S. Holloway
Surface Science Research Centre, University of Liverpool, Liverpool L69 3BX, United Kingdom

A. W. Kleyn
FOM-Institute for Atomic and Molecular Physics, Kruislaan 407, 1098 SJ, Amsterdam, The Netherlands

(Received 22 November 1995; accepted 14 February 1996)

A classical molecular dynamics study is applied to simulate the scattering of NO from Pt(111) in the energy range of 0.3–1 eV. The solid consists of a large number of crystal atoms that interact via an anharmonic nearest-neighbor potential. The NO–Pt(111) interaction potential is constructed as a pairwise additive potential with a well depth of 1 eV for the N end of the molecule towards the surface and purely repulsive for the O end. The in-plane scattering results obtained with this model potential are compared with recent experiments for NO–Pt(111). The angular intensity distributions, the final translational energy, as well as the rotational energy distributions with the corresponding alignment are in qualitative agreement with those experimental results. A detailed examination of the collision dynamics shows that multiple collisions with the surface results predominantly in superspecular scattering. The rotational angular momentum of the scattered molecules exhibits a preference for cartwheeling alignment and the rotational energy distributions for specular and normal exit angles can be described with a Boltzmann distribution, whereas for grazing exit angles they are distinctly non-Boltzmann. The latter structure results from a cutoff in the rotational excitation by the attraction of the well. The high rotational excitation clearly originates from molecules that initially are oriented with the O end towards the surface, whereas for the low rotational excitation this orientation preference disappears. © *1996 American Institute of Physics.* [S0021-9606(96)01819-2]

I. INTRODUCTION

In the last three decades many experiments have provided us with detailed data on the gas-surface interaction.[1] Experimental data comprises of two distinct types of interactions: the ''static'' interaction of adsorption and the ''dynamical'' interaction of scattering processes. Since at equilibrium, adsorbates sit in the potential minimum, static adsorption experiments probe the lowest bound states at the surface and the shape of the potential minimum. Temperature programmed desorption gives information on the binding energy and on the different adsorption states available at the surface. Infrared adsorption spectroscopy, electron energy loss spectroscopy, and inelastic helium scattering measure the vibrational motion and the binding site on the surface of the adsorbed species. Dynamical interactions probed in scattering experiments, on the other hand, take place in the energy range of continuum states and principally yield information on the repulsive part of the interaction potential. Molecular beam experiments determine the energy exchange with the solid and the angular scattering distributions, and as such are a tool to study the form of the lateral interaction potential. Sensitive laser techniques measure the rovibrational state of the scattered molecules and act as a probe of the anisotropy of the interaction potential and also of the coupling of the intermolecular degrees of freedom to others in the system. For spectroscopic reasons, such experiments are particularly well suited to the NO molecule.[2–13]

The measured features resulting from the scattering experiments cannot directly be linked to the potential energy surface. Molecular dynamics (MD) simulations can give insight how those features are connected to properties of the potential energy surface and provide detailed information on the dynamical processes of the gas-surface interaction. Besides rationalizing the experimental results, simulations can bring new light to mechanisms in the scattering dynamics. For the scattering of a diatom, the coupling between the many degrees of freedom make the interaction with the solid rather complicated. Depending on the focus of the research, different models have been applied to simulate the scattering dynamics.[14] Several classical models have been used for NO and CO from metal surfaces,[15–19] to investigate energy exchange with the solid and rotational excitation, whereas a quantum approach has been used to investigate both rotational and vibrational energy exchange with the surface.[20–23]

The present MD simulation was initiated by the results of recent experiments for the rotational excitation of NO

scattered from Pt(111).[24] The interaction of NO with Pt(111) is a paradigm for nonactivated and associative chemisorption. The potential well is deep (about 1 eV) and the orientational anisotropy of the potential energy surface (PES) results in adsorption with the N end towards the surface. Due to the large orientational anisotropy of the PES, one can expect that the molecules at low incidence energies are adiabatically steered into the deep chemisorption well, in a manner that is very reminiscent of dissociative chemisorption of H_2 on transition metals.[25,26]

A simpler system is NO–Ag(111) for which the PES has a shallow physisorption well of about 0.2 eV. The collision dynamics of NO from the Ag(111) surface has been shown to be similar to the collision of a hard ellipsoid.[27,28] The rotational excitation can be modeled by a sudden excitation on the repulsive wall of the PES and the maximum of the derivative of the potential with respect to the orientation angle of the molecule gives rise to a maximum in the rotational excitation, which has been assigned as a rotational rainbow.[2,27,28] These rainbows manifest themselves in a non-Boltzmann behavior of the rotational energy distribution. Quantum and classical calculations have further shown that surface recoil is significant in such experiments and modifies the rainbow positions.[29]

The deep chemisorption well for NO–Pt(111) should lead to quite different dynamical effects. Using a two-dimensional model potential, Harris and Luntz[17] have shown for the very similar CO–Pt(111) system, that all of the degrees of freedom in the system are strongly coupled. The non-Boltzmann distribution in the scattering of CO from Ni(111) is explained as rotational rainbow scattering of the inert side of the CO molecule.[30] Recent experimental observations by Wiskerke *et al.*[31] have exhibited rainbow-like peaks for NO–Pt(111), which appears to be at variance with the model study of Harris and Luntz. If the deep chemisorption well would yield a random redistribution of the energy among all degrees of freedom, a statistical approach should describe the NO–Pt(111) results. The statistical limit, however, does not work.[32] Wiskerke and co-workers proposed a novel two-dimensional model potential facilitating a sudden rotational excitation at the inflection point. In addition to the deep well for the N end oriented towards the surface, a shallow well for the O end was also proposed, with a barrier separating the two.[33] This made the O-end collisions almost inert, resulting in rotational rainbows of molecules that scatter with the O end initially oriented towards the surface.

The present study deploys a molecular dynamics simulation to test if the rainbowlike rotational energy distributions for NO–Pt(111) can be obtained for a high dimensional model of the scattering. We also examine the microscopic origins of the structure to establish whether the term rainbow is at all applicable.

II. COMPUTATION

In the Born–Oppenheimer approximation, the total system is assumed to remain in its electronic ground state during the entire trajectory. However, the NO molecule has an open shell that gives rise to a splitting of the electronic ground state into two spin–orbit states ($^2\Pi_{1/2}$ and $^2\Pi_{3/2}$) and Λ doublets. Only a full quantum calculation can take these effects into account for the scattering dynamics,[23,34–37] but in that case the rather severe restriction of a rigid solid is necessary in order to perform the simulations. Since we use a more realistic model for the solid, only classical mechanics can treat the scattering dynamics due to the many degrees of freedom. The details of the motion on the two electronic surfaces probably has a negligible effect on the outcome of a scattering event and we use this fact to justify the use of a 'mean' potential for the process.

The motions of all particles in the system follow from the numerical integration of the Newton equations, using the Verlet integration algorithm.[38–40] The integration is performed in the Cartesian coordinate system for every particle. The NO trajectory is initiated at a height of 10.6 Å above the surface, where the potential energy is less than 10^{-6} eV. For all simulations, the incidence angle is 45° along the [101] azimuth of the surface; in addition the molecule has no rotational or vibrational energy. Neglecting the lowest quantum rotation for $J=\frac{1}{2}$ for the incidence molecules will not disturb the initial orientation of the molecule, since the time for a full rotation at $J=\frac{1}{2}$ takes about 10 ps, which is much longer than the time the molecule needs to have the first collision with the surface. The crystal atoms are initially at their equilibrium positions for the static surface calculations, or a Maxwell–Boltzmann distribution is used for the initial velocities of the solid to simulate a finite crystal temperature.

III. THE INTERACTION POTENTIALS

The total interaction potential consists of three independent parts describing the interaction between the crystal atoms, the interaction between the NO molecule and the crystal and finally the interatomic interaction between the N and the O in the molecule. The Pt(111) crystal is simulated by 3125 atoms, arranged in the fcc configuration with five (111) planes of 625 atoms. The nearest neighbors interact via an anharmonic interaction potential, that has the form

$$V_c(r)=\tfrac{1}{2}\,k_1(r-d)^2+\tfrac{1}{3}\,k_2(r-d)^3+\tfrac{1}{4}\,k_3(r-d)^4,$$

where r and d are the instantaneous extension and the equilibrium distance between the two nearest neighbors, respectively and k_1, k_2, and k_3 are the force constants. The harmonic force constant follows from the Debye theory and the anharmonicity results from a Taylor expansion of the Lennard-Jones potential. Table I lists the values of the force constants for the surface and the bulk of the Pt(111) crystal. The values of the force constants taken for the surface atoms are about 20% lower than those for the bulk, in order to reproduce the lower surface Debye temperature.[41,42]

The interaction potential between the NO molecule and the Pt(111) crystal is also taken to be pairwise additive, where the N and the O atoms interact individually with every crystal atom. As a starting point, we choose the functional form for the NO–Pt(111) interaction similar to that introduced by Muhlhausen *et al.*,[18] which was originally designed

TABLE I. The values of the parameters for the interaction potential between the crystal atoms, for the NO–Pt(111) interaction and for the internal potential of the NO molecule. The two values for the force constants of the crystal potential are for the bulk (left) and surface (right). The other potential parameters are taken from Ref. 18, although the value for B is modified to yield a well of 1 eV. The distance and energy units are in Ångström and electronvolts, respectively.

k_1	6.875	1.573
k_2	−26.043	−5.957
k_3	55.329	12.656
A	634.5	
α	3.366	
B	0.748	
β	1.683	
r_e	1.5	
F	6.618	
κ	2.743	
R_{NO}^{eq}	1.15	

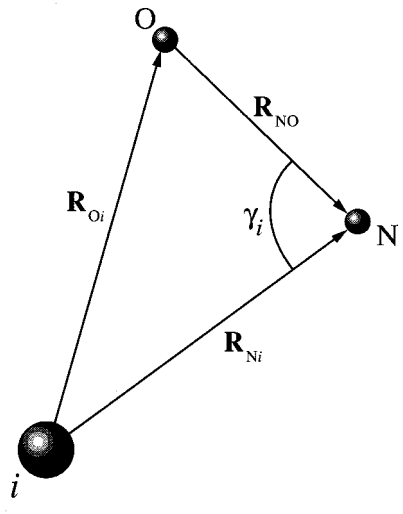

FIG. 1. A sketch of the vectors and the orientation angle for the NO molecule interacting with a single crystal atom, as it is used for the interaction potential in Eqs. (1) and (2).

to describe the interaction between NO and Ag(111). In hindsight because their well depth was 1 eV rather than the observed 0.2 eV, the PES is probably more appropriate for NO–Pt(111). In modified form, it was also used by Jacobs and Zare,[19] however, since it did not reproduce the energy dependence of the sticking probability,[43] we have therefore further modified it to achieve a higher sticking probability. The width of the well with respect to the orientation angle of the molecule is enlarged by decreasing the power for the cosine term of the orientation angle. In this way more orientations will lead to scattering in the well, which in turn enhances the sticking probability.[17] Since the molecule does not adsorb with the O end towards the surface,[44,45] the interaction with the O end of the molecule is taken to be purely repulsive. The interaction potential between the NO molecule and a single Pt atom is described by

$$V_{\mathrm{NO-Pt}}(R_{Oi},R_{Ni},\cos\ \gamma_i) = Ae^{-\alpha R_{Oi}} + B[(e^{-\beta(R_{Ni}-r_e)}+\cos\ \gamma_i)^2-\cos^2\ \gamma_i], \quad (1)$$

with

$$R_{Oi}=|\mathbf{R}_{Oi}|=|\mathbf{R}_O-\mathbf{r}_i|,$$

$$R_{Ni}=|\mathbf{R}_{Ni}|=|\mathbf{R}_N-\mathbf{r}_i|,$$

$$R_{NO}=|\mathbf{R}_{NO}|=|\mathbf{R}_N-\mathbf{R}_O|,$$

$$\cos\ \gamma_i=\frac{\mathbf{R}_{Ni}\cdot\mathbf{R}_{NO}}{R_{Ni}R_{NO}},$$

where $\mathbf{R}_N$, $\mathbf{R}_O$, $\mathbf{r}_i$ are the position vectors of the N, O and crystal atom i, respectively, γ_i is the orientation angle between the NO and the line that connects the N atom with crystal atom i. Figure 1 illustrates the vectors and the orientation angle for the potential. The O end interaction is simply an exponential repulsion, whereas the N-end interaction is a Morse potential for $\cos\ \gamma_i<0$, that turns into an exponential repulsion for $\cos\ \gamma_i\geqslant 0$.

The potential parameters listed in Table I, yield the PES of Fig. 2. The transition from repulsion to attraction for the O-end and the N-end pointing towards the surface, results in a large orientational anisotropy, when compared to previous studies. The well depth for the atop site is −0.98 eV, located at 2.1 Å above the surface and for the center site −0.84 eV at 2.0 Å. This implies that the NO adsorbs at the atop site, which is in agreement with the very similar CO–Pt(111) system.[46,47] A recent low energy electron diffraction (LEED) study on NO–Pt(111) has shown that NO adsorbs at the center site on an NO covered surface;[44] for a clean surface, the adsorption site has not been determined accurately by LEED. Since earlier studies of NO adsorption on Pt(111) indicated a change in binding site with coverage,[11] adsorption of NO perpendicular at the atop site cannot be excluded. The diffusion barriers for CO on Pt(111) have been determined to be around 0.2 eV,[46,47] which compares reasonably well with our value of 0.14 eV.

It is noteworthy that the orientational anisotropy in our potential is very large. The difference between the molecular center of mass and the surface for the two upright orientations of the molecule at the repulsive energy of 0.1 eV is about 1.5 Å. This is almost a factor of 10 larger than for the potential proposed by Wiskerke *et al.*[31] for NO–Pt(111) or the Voges and Schinke potential for NO–Ag(111).[27] The potential for the latter system by DePristo and Alexander[36] yields a distance of about 1 Å. The enormous anisotropy in Fig. 2 will be shown to give rise to facile rotational excitation and chattering. It is also noteworthy that the anisotropy of the potential around the N end is rather low.

Finally, a Morse potential, fitted to the gas-phase NO molecule, describes the internal potential of the molecule

$$V_{NO}(R_{NO})=F[(e^{-\kappa(R_{NO}-R_{NO}^{eq})}-1)^2-1], \quad (2)$$

where R_{NO} is the instantaneous intermolecular distance and R_{NO}^{eq} is the equilibrium distance.

Above 5 eV, the PES in Fig. 2 permits the molecule to penetrate between the crystal atoms at the center site. We appreciate that this is quite unrealistic but have only em-

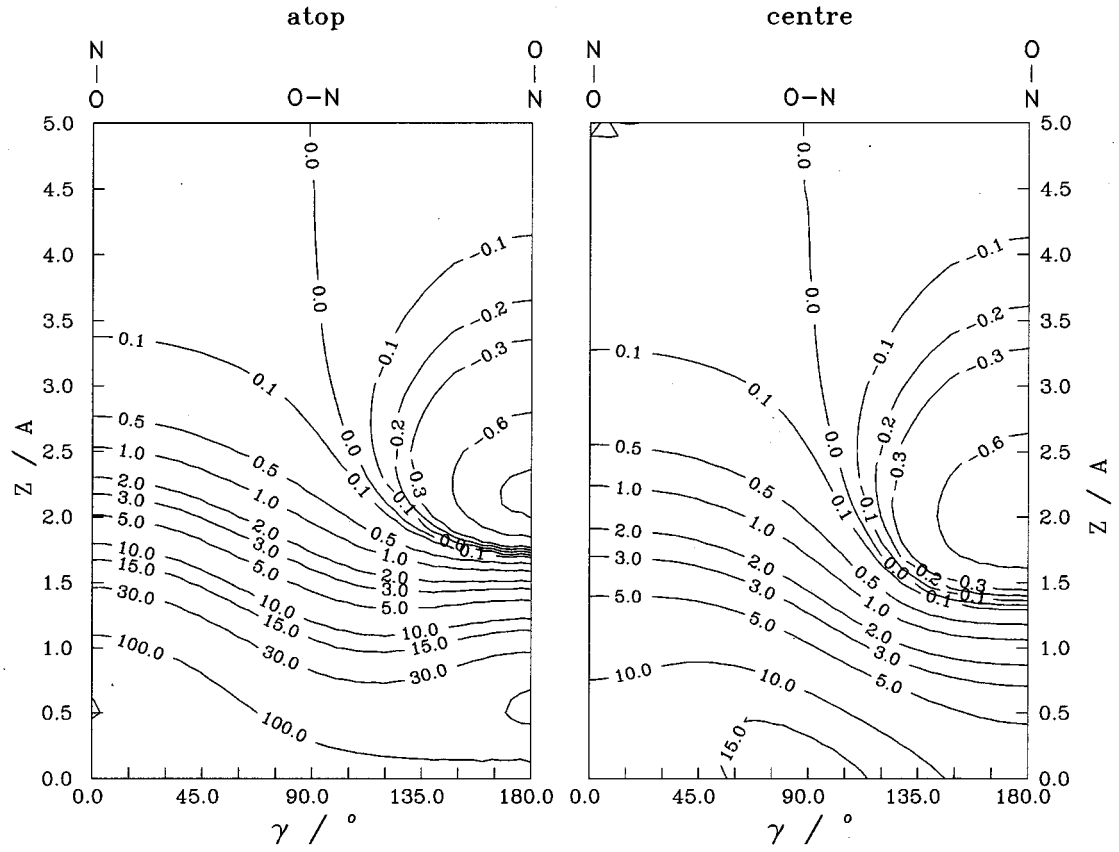

FIG. 2. The contour plots of the static NO–Pt(111) potential energy surface at the atop and center sites. Z is the distance between the center of mass of the NO molecule and the plane containing the centres of the Pt surface atoms. γ_s is the orientation angle of the molecule with respect to the surface normal. The contour values are in electronvolts.

ployed the model for lower incidence energies. It is noteworthy that for more than 50% of all molecular orientations the PES is purely repulsive. For such a PES to yield a large sticking probability requires extensive steering of the molecule in order to reach the deep chemisorption well.

IV. ANGULAR AND KINETIC ENERGY DISTRIBUTIONS

The experimental data in Fig. 3(a) show very broad angular distributions for in-plane scattering of NO from Pt(111). Their noncosine nature indicates that specular scattering dominates. The mean final translational energy is almost independent of the outgoing angle, whereas the mean rotational energy slightly increases with increasing final angle.[31,48] Comparing these results to those for a simple physisorption system such as Ar–Ag(111) (Ref. 49) and Ar–Pt(111) (Ref. 50), shows remarkable differences. The angular width for NO–Pt(111) is much larger and, compared to the rare gases, the energy transfer shows only a small angular dependence. The relative insensitivity for those parameters of the present system is a good indicator that the dynamics must be significantly different. The high trapping probability and the coupling between translation and rotations could result in energy exchange between the many degrees of freedom which cannot easily be explained by assuming the molecule to be inert.

Figures 3(c)–3(f) show the results for our MD simulation for the potential described earlier to compare with the experimental results. In the analysis, the binning for the outgoing angle θ_f is 5° and the constant solid angle of the detection window is included in order to detect only in-plane scattered molecules, as done in the experiments. To improve the statistics, the acceptance window is taken to be much larger than in the experiments, i.e., 3×10^{-2} st vs 4×10^{-5} st. The simulated angular distributions are normalized to the same incidence flux and are plotted on the same relative scale. The increase of peak intensity observed with increasing energy is due to a decrease of the sticking probability. The maxima of the angular intensity distributions for the experiment and the simulations are scaled to have equal values at the maximum. The shapes of the angular intensity distributions from experiment and simulation are very similar and the final kinetic energy also shows the same trend as in the experiments. The simulations at a finite temperature of 600 K show a satisfactory agreement with the experimental results at a slightly lower temperature of 475 K.

The influence of the surface motion on the scattering

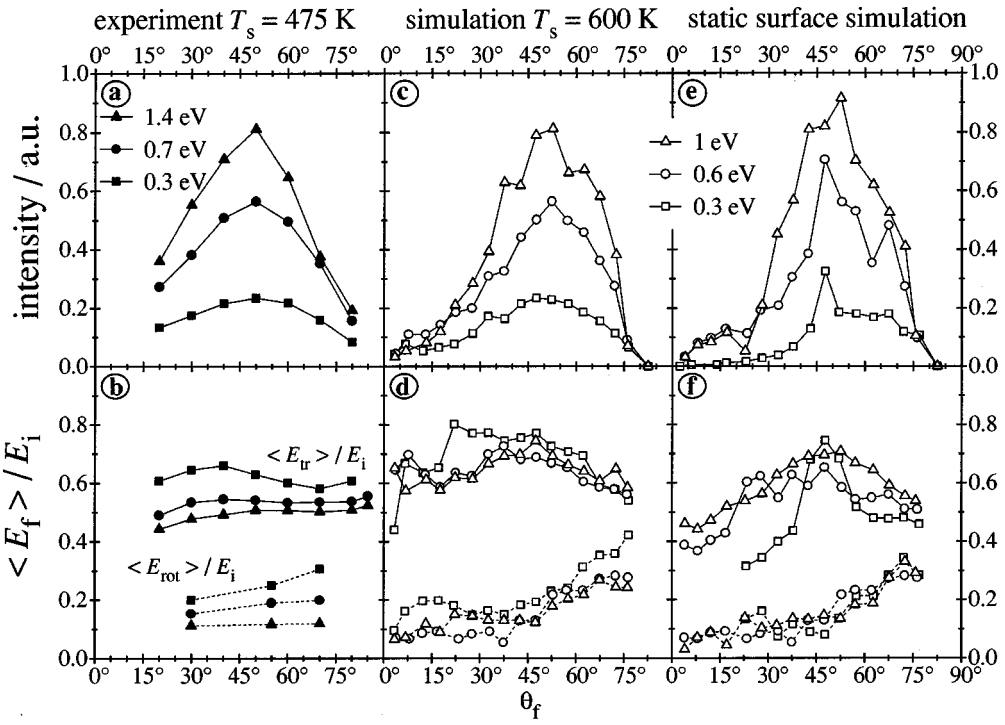

FIG. 3. A comparison between the experimental results (Ref. 31) and the present simulations. The angular intensity distributions and mean final energy are displayed for in-plane scattering of NO from Pt(111), impinging at an angle of 45° and three incidence energies. The experimental results in panel (a) are scaled to the simulations in panel (c) to have equal value in the maximum. The intensity distributions for the simulations are normalized to the incoming flux. In the lower panels the mean translational and rotational energy is shown, scaled to the incidence translational energy.

dynamics may be understood by comparison with an additional simulation using a static surface. For $E_i = 0.3$ eV, the angular intensity distribution for the static surface shows a decrease for the scattering towards the surface normal when compared with a 600 K surface. For the higher incidence energies, the influence of the surface temperature is small, yielding similar angular distributions in panels (c) and (e) in Fig. 3. Since even for the static surface the angular distributions are very broad, the thermal vibrations of the surface atoms appear not to be the origin. In contrast, the surface temperature has a considerable effect on the final translational and rotational energies. For the static surface, the mean final translational energy of $E_i = 0.3$ eV depends strongly on the site of impact at the surface. The high translational energy in the specular peak at $\theta_f = 45°$ is a result from scattering around the centre site, because for such an interaction, the molecule interacts simultaneously with three Pt atoms and the energy transfer to the solid is relatively low. This site effect vanishes for increasing incidence energy. Since molecules scattered from the static surface cannot gain energy from the surface atoms, for the 600 K surface, the increased mean final translational energies must arise from the vibrating surface atoms. This effect tends to smooth the curves as seen in panel (a) of Fig. 3. The effect of the temperature on the mean rotational excitation is different. At the lowest incidence energy of 0.3 eV for scattering subspecular ($\theta_f < 30°$) and superspecular ($\theta_f > 60°$), the surface temperature of 600 K causes an increase of the mean rotational energy. For other situations the surface temperature hardly affects the rotational excitation or only causes a minute increase.

The strong interaction between the NO and the Pt(111) surface, in particular, the strong orientational anisotropy, increases the probability for the molecule to have multiple collisions with the surface. In the simulations, the multiple collisions are registered when more than one sign change takes place in the perpendicular velocity component of the centre of mass. Figure 4 shows the contributions of the multiple collisions for the scattering from a surface of 600 K. The angular intensity distributions show that the multiply colliding molecules scatter preferentially to large exit angles, indicating a slow relaxation of the parallel component of the momentum. The relaxation of the perpendicular component of the momentum is very fast (within 2 or 3 collisions), which has also been seen previously for simulations of rare gas scattering.[49,51,52] The relative contribution of multiple collisions to the total scattering distributions decreases with increasing energy. Comparing final energies as a function of the outgoing angles for the single and multiple collisions in Fig. 4, we see that the mean final translational and rotational energies are very similar and thus the energy exchange for the NO molecule is dominated by the final encounter with the surface, remembering its parallel component of the incoming velocity.

Employing the same analysis as applied in previous work for the total scattering distributions[53] shows that the out-of-plane angular width keeps pace with its in-plane counterpart. The in-plane width ranges from 36° to 30° as the

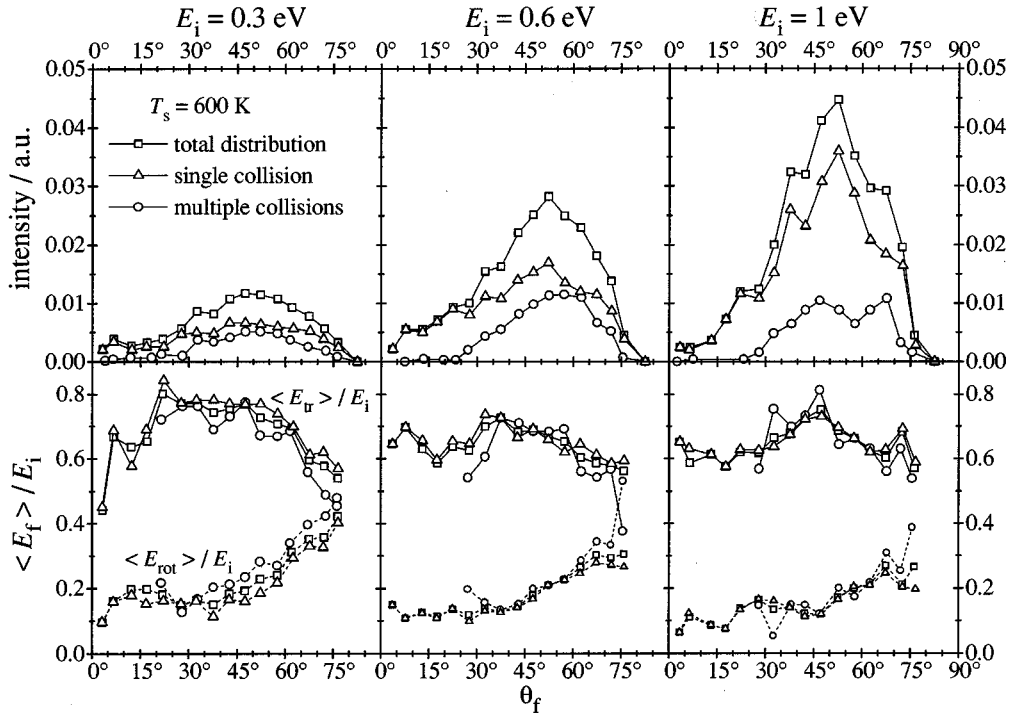

FIG. 4. The contribution of the multiple collisions to the angular intensity distributions and the mean final translational and rotational energy for NO scattering from a Pt(111) surface with a temperature of 600 K impinging at an angle of 45°. All intensity distributions are normalized to the incoming flux.

energy increases from 0.3 to 1 eV, while the out-of-plane width decreases from 40° to 33° (when taken through the centroid of the intensity distribution). Simulating an in-plane slit of $|\Delta\phi_f|<2°$, about 10% scatters in the in-plane direction for $E_i=0.3$ eV and increases to 13% for 1 eV. Due to the broad angular widths, this value is lower than for the scattering of Ar from Ag(111).[53]

V. ROTATIONAL EXCITATION

The mean rotational excitation shown in Fig. 3 varies as a function of the outgoing angle in a way that is consistent with experimental results. The experimental results for the rotational energy distribution for three outgoing angles in Fig. 5 show that almost all data can be described by Boltzmann distributions. For the lowest incidence energy at grazing exit, rotational excitation has a distinctly non-Boltzmann appearance. Wiskerke *et al.* attributed the non-Boltzmann behavior to rotational rainbow scattering.[31,33]

To investigate the rotational excitation within our simulations, we examined the rotational energy distribution for a 600 K surface at three distinct regions of the final scattering angles: subspecular at $\theta_f<30°$, scattering in the specular direction, $30°<\theta_f<60°$, and finally superspecular at $\theta_f>60°$. In each region the rotational energy is binned into energy levels of $J(J+1)B$, where J is the rotational quantum number and B the rotational constant (2.11×10^{-4} eV for NO). In order to get reasonable statistics, the accepted scattering solid angle is enlarged to 0.82 st, with θ_f in the range as indicated. To simulate a constant window opening, the out-of-plane angle ϕ depends on the in-plane angle θ: $\Delta\phi=\Delta\phi_{(\theta=90°)}/\sin\theta$. The results of the simulations are shown in Fig. 5. For almost all incidence conditions a Boltzmann-type rotational energy distribution is found, the exception being scattering at grazing exit for the low incidence energies. The corresponding temperatures of the rotational energies for the molecules scattered subspecularly, are

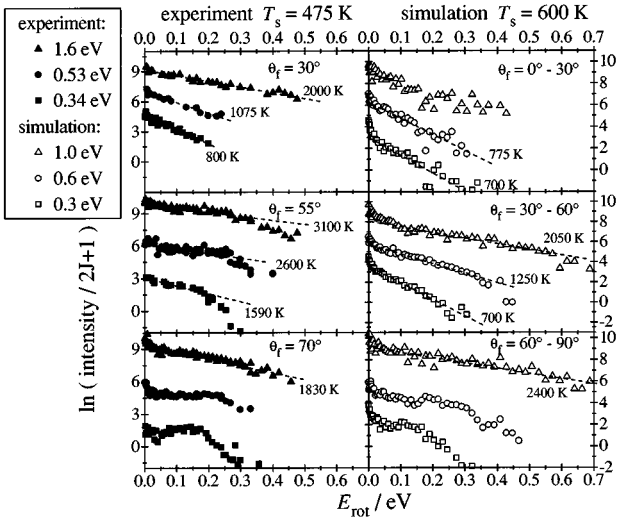

FIG. 5. Boltzmann plots of the rotational energy distribution for NO scattered from Pt(111) with an incidence angle of 45°. The left panels contain the experimental data (Ref. 31) and right panels the corresponding simulations. The indicated temperatures result from the linear least square fit through the data points and θ_f indicates the θ window for the exit angles.

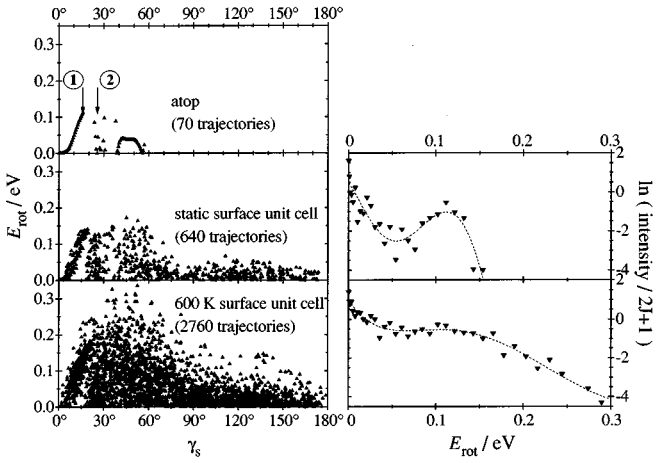

FIG. 6. The left panels show the final rotational excitation as a function of the initial orientation angle γ_s of the molecule (γ_s is defined with respect to the surface normal). The initial incidence energy is 0.3 eV. The impact site of the molecule is at the atop site (with a static surface) and the entire surface unit cell for both the static surface and the 600 surface. For the atop site, sticking occurs for all molecules with orientation angles beyond 60°. The adjacent right panels show the corresponding Boltzmann plots for the rotational energy distributions. The lines through the Boltzmann plots are merely a guide of the eye. The numbers 1 and 2 for the atop scattering correspond to the two trajectories in Fig. 7.

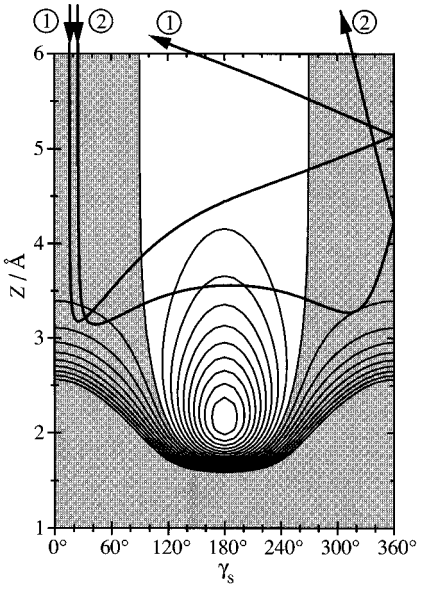

FIG. 7. Two trajectories are depicted in the contour plot of the atop potential of Fig. 2. The incidence energy and angle are 0.3 eV and 45°. Trajectory 1 has an initial orientation angle of 16°, which leads to a high final rotational energy. For trajectory 2 the initial orientation angle is 25°, resulting in the rotational cutoff by the attraction into the well. The shaded region indicates the repulsive part of the interaction potential. The spacing between the contour lines is 0.1 eV.

for the simulations about 700 K (≈0.06 eV). This indicates that the coupling between rotation and translation in this angular range is rather weak. There are essentially no experimental results in this angular range. Experimental results at 30° show already an increase of the Boltzmann temperatures with increasing incidence energy, similar to that seen in the simulations around the specular angle. The effective temperatures of the Boltzmann distributions for scattering in the specular direction increase with the incidence energy, implying a stronger coupling between the rotation and the translational energy.

Most of the rotational scattering distributions in Fig. 5 show a Boltzmann-like behavior. Taatjes *et al.* have demonstrated that the majority of the data could be described using statistical models.[32] This is remarkable since the interaction time with the surface (≈ps) is quite short for some kind of pseudoequilibration. It is rather scrambling of rotational and translational energy leading to chattering (see the following) that cause the rotational Boltzmann distribution. In spite of this, a non-Boltzmann distribution survives for the molecules with low energies and at grazing exit. Figure 6 elucidates the mechanism for this rotational energy distribution. Scattering only from the atop site, yields the rotational energy as a function of the orientation angle of the molecule, as drawn in the uppermost panel of Fig. 6. Beginning at $\gamma_s=0°$ the rotational energy increases with increasing angle since the torque on the molecule is gradually becoming larger (see the contour plot in Fig. 2). For orientation angles beyond that yielding the maximum rotational energy (at $\gamma_s\approx16°$), the torque on the molecule still increases, but this does not give rise to a larger rotational energy for the scattered molecules. On the contrary, the rotational energy decreases. The present maximum arises as a result of the competition between the repulsive collision (scattering the molecule away from the surface) and the torque (turning the molecule into the deep well). If the angular momentum is not too large, the molecule is already far away from the surface before the orientation with the N end down experiences the deep potential well. On the other hand, when the angular momentum is large, the molecule spins into the deep well while it is still close to the surface. Now the attractive force of the well hinders the rotation and chattering reduces the final rotational excitation. This mechanism causes a rotational quenching before the maximum torque in the first collision is reached. The rotational excitation followed by deexcitation effectively steers the molecule into the deep chemisorption well. Figure 6 further shows that even when scattering from the static surface unit cell is considered, the rotational cutoff still survives and the corresponding plot shows very clearly that the cutoff leads to a very strong non-Boltzmann behavior for the rotational energy distribution. For a surface temperature of 600 K, the final rotational energy is yet still more randomized by the motion of the surface atoms and though the cutoff in the rotational energy shifts upwards, it is still present, as evidenced by the nonlinearity in the Boltzmann plot.

The mechanism to explain the non-Boltzmann distribution of the rotational energy, is shown in Fig. 7 for two trajectories scattering from the atop site. One trajectory results in high rotational excitation just before the rotational cutoff. It is a sudden rotational excitation at the classical turning point and though the trajectory is slightly refracted by the well, the molecule can freely rotate and escape. The

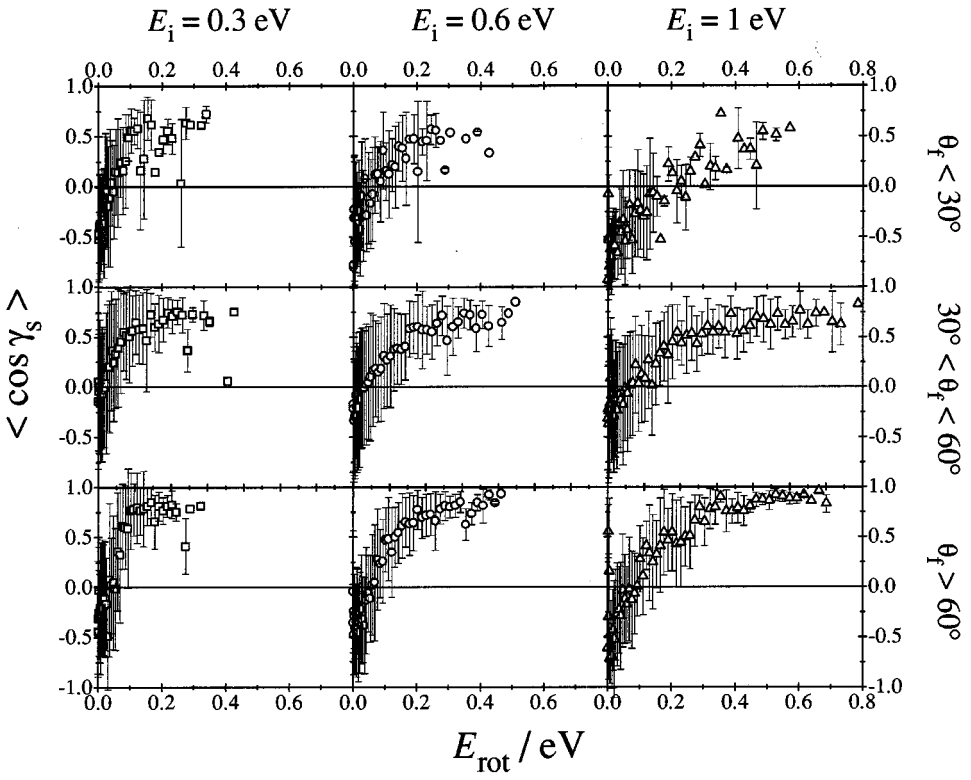

FIG. 8. Mean initial orientation angle of the molecule as a function of the rotational energy. The upper panels contain the subspecular, the center panels the specular, and the lower panels the superspecular scattered molecules. $\langle \cos \gamma_s \rangle = 1$ corresponds to the O end and $\langle \cos \gamma_s \rangle = -1$ to the N end oriented towards the surface. The error bars are the statistical spread after averaging.

second trajectory receives a larger torque at the reflection point, rotates through the well and experiences an opposite torque. The resulting chattering reduces the rotational excitation. Although the rotational cutoff leads to non-Boltzmann energy distributions, it is hard to assign this peak to be a rotational rainbow. A suppression of rainbows by the presence of an attractive well has been shown previously for atom scattering.[54] As shown by Horn *et al.*,[55,56] it is difficult to identify a rainbow in the case of a differential cross section of a higher dimensionality. A proper analysis can only be carried out for a calculation involving a static lattice with no recoil and such an analysis has not been carried out here.

The temperatures resulting from the Boltzmann plots in Fig. 5 are at variance with the mean rotational energies in Fig. 3(d). If the rotational energy were exactly a Boltzmann distribution, the mean rotational energy would correspond to the rotational temperature. However, Fig. 5 shows a high density of the lowest rotational states that do not follow the Boltzmann distribution and this causes a difference between the mean rotational energy and the rotational temperature. The fraction of molecules contributing to the lowest rotational energies turns out to be exceedingly large. In order to get insight which classes of trajectories contribute to the different rotational energy levels, we plot in Fig. 8 the mean initial orientation angle as a function of the final rotational energy. The higher rotational energies clearly originate from collisions of the molecules with the O end initially oriented towards the surface ($\langle \cos \gamma_s \rangle \approx 1$), which is agreement with experimental results.[24,57] However, the statistical spread at low rotational energies indicates that many orientation angles contribute, including those with the N end towards the surface. These latter molecules scatter through the deep potential well resulting in a low rotational excitation. The enhanced intensity of the lowest rotational energies thus has its origin in the scattering of molecules with the N end directed towards the surface, that are capable of escaping from the deep well via scattering at the center site.[58] These are the trajectories in Fig. 6 of the 600 K surface with $\gamma_s > 90°$.

The rotational alignment parameter $A_0^{(2)}$ is a measure of the orientation of the angular momenta of the scattered molecules with respect to a symmetry axis.[59–61] Choosing the surface normal as this, we disregard the azimuthal dependence of the crystal symmetry. Then the alignment in the classical limit is defined as

$$A_0^{(2)}(J) = \frac{1}{N_J} \sum_{i \in [J]} (3 \cos^2 \vartheta_f - 1),$$

where the summation is over all molecules in $[J]$, which is the bin containing the molecules having quantum number J, N_J is the number of molecules in $[J]$, and ϑ_f is the angle between the final angular momentum of the NO molecule and the surface normal. $A_0^{(2)} = 2$ corresponds to helicopter rotation, whereas $A_0^{(2)} = -1$ corresponds to cartwheeling and

when $A_0^{(2)}=0$ the rotational distribution is isotropic. The alignment for the data in Fig. 8 is isotropic for all scattered molecules with a rotational energy below $J=35$ ($E_{\mathrm{rot}}=0.27$ eV). For higher rotational energies, the alignment changes to preferentially cartwheels. This behavior also has been seen experimentally by Jacobs *et al.*[12,19] The isotropic distribution is found to result from a mixture of molecules oriented initially with O end and N end towards the surface, whereas the cartwheeling molecules originate predominantly from orientations with the O end towards the surface.

VI. VIBRATIONAL EXCITATION

The model potential also allows the molecule to vibrate, but the excitation in the simulations remains so low, that essentially all molecules would scatter in their vibrational ground state. Experiments have also shown that the vibrational excitation cross section for NO–Pt(111) in the energy regime investigated here has a very low probability.[13] In the simulations we observe that during the collision with the surface, the NO bond relaxes adiabatically under the influence of the interaction with the surface and therefore no vibrational excitation occurs.

VII. STICKING

All trajectories are initiated at approximately 10 Å above the surface. Molecules not reappearing at this height after collision, are assumed to be stuck. This definition is clearly an overestimate for the sticking probability, since it includes molecules that make more than ten collisions with the surface or come in the neighborhood of the edge atoms of the surface. Both situations occur in the calculations within 10 ps, which in itself is quite short to define a molecule to be stuck. The resulting sticking probability is shown in Fig. 9. In spite of the purely repulsive O end, the sticking tends to unity in the low energy regime. This indicates that rotationally mediated adsorption (RMA) occurs: rotational excitation followed by chattering steers the molecules almost adiabatically to the bottom of the chemisorption well. However, the absolute value of the sticking probability is still too low at higher incidence energies. Nevertheless, the sticking probability obtained on our modified PES becomes a factor of 3 larger than that used by Muhlhausen *et al.*[18] As mentioned earlier, the main difference between the two model potentials is the broadening of the potential well with respect to the orientation angle of the molecule and this must therefore account for the enhanced sticking.

Figure 6 clearly shows that for the atop collision, all molecules oriented with the N end towards the surface ($\gamma_s \geqslant 90°$) stick, but this is not the case for scattering across the entire unit cell. This means that site dependent sticking occurs (as also observed in Ref. 19). A low sticking probability around the center sites is partly the reason for the low sticking in Fig. 9 and thus the contribution to the scattering distributions of the N-end orientations is overestimated in our simulations, which on its turn causes a ''pollution'' of all scattering distributions, especially of the rotational non-Boltzmann distributions at superspecular exit angles.

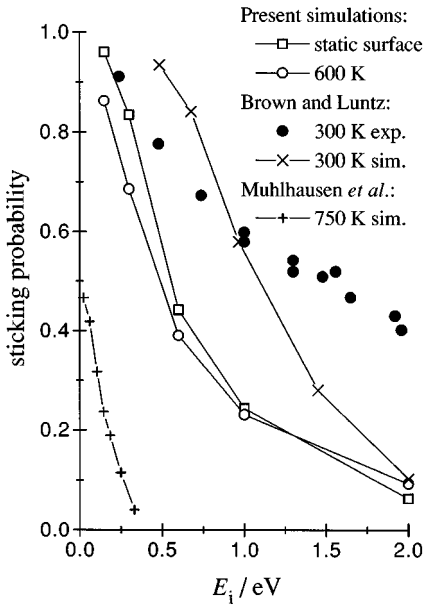

FIG. 9. The sticking probability for the present NO–Pt(111) simulations with an incidence angle of 45° as a function of the incidence energy, compared with the results of the simulations by Mulhausen *et al.* (Ref. 18) (incidence angle of 50°) and by Brown and Luntz (Ref. 43) (incidence angle of 60° for experiment and normal incidence for the simulations).

Another reason for the low sticking probability is the purely repulsive interaction when the O end of the molecule is oriented towards the surface, since molecules maintaining that orientation will never stick, irrespective of impact parameter. We note that the CO–Pt potential used by Harris and Luntz[17] and presumably also the NO–Pt potential used by Brown and Luntz[43] has a well for the O end of the molecule, albeit less deep than for the C or N end. However, there is no spectroscopic evidence whether the O end of the molecule has a well or not. This point could be settled by ab initio total energy calculations.

Looking at the mean initial orientation of the molecules that stick, its value is a few percent in favor of the N-end orientation and this is broadly in accord with experimental measurements.[62,63] That means that even the repulsive O-end orientations lead to sticking. This can only occur for O-end down with the molecule tilted (statistically pure O end and pure N end have zero probabilities). The molecule now looses translational energy into rotation, which partly leads to sticking. However, at closest approach the deep well prevents the molecules from fully rotating while at the surface. The molecules either rotate in a frustrated mode or indeed make a full rotation but then escape as soon as the pure repulsion from the O end pushes the molecule away from the surface. If the O end would not be purely repulsive, the effect of RMA would most presumably be stronger, because the rotational deexcitation at the O end could be less efficient. This is why the calculations by Brown and Luntz show a slower fall off with energy than our calculations.

VIII. CONCLUSION

A molecular dynamics simulation, applying an empirical model potential has been used to simulate the scattering dynamics of NO from Pt(111) for incidence energies between 0.3 and 1 eV. Results agree qualitatively well with the experiments, particularly the broad angular distributions, the final translational energy and the rotational excitation as a function of the incidence energy.

The simulations show that it is the strong interaction between the molecule and the surface atoms that results in the broad angular distributions, and not the thermal broadening by the finite surface temperature, although thermal vibrations do affect the translational energy and increase the rotational excitation for the lowest incidence energy. An analysis of the behavior of the molecules that make multiple collisions with the surface, shows that those molecules scatter preferentially superspecular. However, the energy exchange with the surface is not affected by these multiple collisions, leading to the conclusion that the last collision with the surface determines the final energy of the scattered molecule.

In agreement with experiments, the final rotational energies show Boltzmann distributions, except for scattering at superspecular exit angles. The pseudoequilibration indicates a large scrambling of the energy over the molecular degrees of freedom and since the influence of the surface temperature is not so large, the statistical behavior is due to the collision dynamics. In fact, chattering frequently occurs and leads to the quasistatistical or Boltzmann character of the rotational state distributions. The simulated non-Boltzmann distributions result from a rotational cutoff due to the strong orientational anisotropy and the deep well of the interaction potential and is not a result of an extreme of the torque on the molecule at the reflection point.

The initial orientation of the molecule is crucial in determining the final rotational energy. The maximum rotational excitation occurs at the classical turning point and thus the dynamics for the inert O end is different than for the N end. The highly rotation excited molecules originate from collisions with the O end initially oriented towards the surface and are characterized by a cartwheeling rotation. The sticking probability shows the correct trend in the low energy regime, however, at higher energies, it is still too low compared to experimental data. This might be due to the purely repulsive nature of the O end in the present simulations.

ACKNOWLEDGMENTS

This work is part of the research program of the ''Stichting voor Fundamenteel Onderzoek der Materie'' (FOM), that is financially supported by the ''Nederlandse Organisatie voor Wetenschappelijk Onderzoek'' (NWO). The collaboration between Amsterdam and Liverpool is supported by the E.C. Science Program ERBSCI*CT910721. All calculations have been performed on an 8 node SP1 system from IBM installed at the Academic Computing Services Amsterdam (SARA). We thank SARA, the two universities in Amsterdam, the Stichting Mathematisch Centrum and IBM Netherlands for providing access to the system.

[1] *The First Thirty Years*, edited by C. B. Duke (Elsevier, The Netherlands, 1994); Surf. Sci. **299/300** (1994).
[2] F. H. Geuzebroek, A. E. Wiskerke, M. G. Tenner, and A. W. Kleyn, J. Phys. Chem. **95**, 8409 (1991).
[3] A. W. Kleyn, A. C. Luntz, and D. J. Auerbach, Surf. Sci. **117**, 22 (1982).
[4] J. Misewich, H. Zacharias, and M. M. T. Loy, Phys. Rev. Lett. **55**, 1919 (1985).
[5] C. T. Rettner, F. Fabre, J. Kimman, and D. J. Auerbach, Phys. Rev. Lett. **55**, 1904 (1985).
[6] H. Vach, J. Häger, and H. Walther, J. Chem. Phys. **90**, 6701 (1989).
[7] A. Mödl, T. Gritsch, F. Budde, and G. Ertl, Phys. Rev. Lett. **57**, 384 (1986).
[8] K. Fukutani, Y. Murata, R. Schwarzwald, and T. J. Chuang, Surf. Sci. **311**, 247 (1994).
[9] H. Müller, G. Zagatta, N. Böwering, and U. Heinzmann, Chem. Phys. Lett. **223**, 197 (1994).
[10] R. J. Hamers, P. L. Housten, and R. P. Merrill, J. Chem. Phys. **83**, 6045 (1985).
[11] D. S. King and R. R. Cavanagh, Adv. Chem. Phys. **76**, 45 (1989).
[12] D. C. Jacobs, K. W. Kolasinski, S. F. Shane, and R. N. Zare, J. Chem. Phys. **91**, 3182 (1989).
[13] M. Asscher, W. L. Guthrie, T. H. Lin, and G. A. Somorjai, J. Chem. Phys. **78**, 6992 (1983).
[14] R. B. Gerber. Chem. Rev. **87**, 29 (1987).
[15] J. C. Polanyi and R. J. Wolf. J. Chem. Phys. **82**, 1555 (1985).
[16] G. D. Billing. Chem. Phys. **86**, 349 (1984).
[17] J. Harris and A. C. Luntz, J. Chem. Phys. **91**, 6421 (1989).
[18] C. W. Muhlhausen, L. R. Williams, and J. C. Tully, J. Chem. Phys. **83**, 2594 (1985).
[19] D. C. Jacobs and R. N. Zare, J. Chem. Phys. **91**, 3196 (1989).
[20] J. Kimman, C. T. Rettner, D. J. Auerbach, J. A. Barker, and J. C. Tully, Phys. Rev. Lett. **57**, 2053 (1986).
[21] C. Haug, W. Brenig, and T. Brunner, Surf. Sci. **265**, 56 (1992).
[22] G. A. Gates, G. R. Darling, and S. Holloway, J. Chem. Phys. **101**, 6281 (1994).
[23] D. Lemoine, J. Chem. Phys. **101**, 4350 (1994).
[24] A. E. Wiskerke, C. A. Taatjes, A. W. Kleyn, R. J. W. E. Lahaye, S. Stolte, D. K. Bronnikov, and B. E. Hayden, J. Chem. Phys. **102**, 3835 (1995).
[25] M Kay, G. R. Darling, S. Holloway, J. A. White, and D. M. Bird, Chem. Phys. Lett. **245**, 311 (1995).
[26] A. Gross, S. Wilke, and M. Scheffler, Phys. Rev. Lett. **75**, 2718 (1995).
[27] H. Voges and R. Schinke, Chem. Phys. Lett. **100**, 245 (1983).
[28] M. G. Tenner, E. W. Kuipers, A. W. Kleyn, and S. Stolte, Surf. Sci. **242**, 376 (1991).
[29] M. R. Hand, X. Y. Chang, and S. Holloway, Chem. Phys. **147**, 351 (1990).
[30] M. A. Hines and R. N. Zare, J. Chem. Phys. **98**, 9134 (1993).
[31] A. E. Wiskerke, C. A. Taatjes, A. W. Kleyn, R. J. W. E. Lahaye, S. Stolte, D. K. Bronnikov, and B. E. Hayden, Chem. Phys. Lett. **216**, 93 (1993).
[32] C. A. Taatjes, A. E. Wiskerke, and A. W. Kleyn, J. Chem. Phys. **102**, 3848 (1995).
[33] A. E. Wiskerke, C. A. Taatjes, A. W. Kleyn, R. J. W. E. Lahaye, S. Stolte, D. K. Bronnikov, and B. E. Hayden, Faraday Disc. **96**, 296 (1993).
[34] D. Lemoine and G. C. Corey, J. Chem. Phys. **92**, 6175 (1990).
[35] B. Pouilly, J. M. Robbe, and D. Lemoine, J. Phys. Condens. Matt. **6**, 9689 (1994).
[36] A. E. DePristo and M. H. Alexander, J. Chem. Phys. **94**, 8454 (1991).
[37] M. H. Alexander, J. Chem. Phys. **94**, 8468 (1991).
[38] L. Verlet, Phys. Rev. **159**, 98 (1967).
[39] S. E. Koonin, *Computational Physics*, 1st ed. (Benjamin/Cummings, Menlo Park, CA, 1986), Chap. 3.1, p. 50.
[40] M. P. Allen and D. J. Tildesley, *Computer Simulations of Liquids*, 1st ed. (Oxford University Press, New York, 1987), Chap. 3.2.1, p. 78.
[41] D. P. Jackson. Surf. Sci. **43**, 431 (1974).
[42] G. A. Somorjai, *Introduction to Surface Science and Catalysis*, 1st ed. (Wiley, New York, 1994), Chap. 4.2.3, p. 319.
[43] J. K. Brown and A. C. Luntz, Chem. Phys. Lett. **204**, 451 (1993).
[44] N. Materer, A. Barbieri, D. Gardin, U. Starke, J. D. Batteas, M. A. Van Hove, and G. A. Somorjai, Surf. Sci. **303**, 319 (1994).
[45] D. R. Jennison, E. B. Stechel, A. R. Burns, and Y. S. Li, Nucl. Instrum. Meth. B **101**, 22 (1995).
[46] M. Croci, C. Felix, G. Vandoni, W. Harbich, and R. Monot, Surf. Sci. **290**, L667 (1993).

[47] G. Hähner, J. P. Toennies, and C. Wöll, Appl. Phys. A **51**, 208 (1990).
[48] A. E. Wiskerke and A. W. Kleyn, J. Phys. Condensed Matt. **7**, 5195 (1995).
[49] R. J. W. E. Lahaye, A. W. Kleyn, S. Stolte, and S. Holloway, Surf. Sci. **338**, 169 (1995).
[50] M. Persson and C. T. Rettner (private communication).
[51] M. Head-Gordon, J. C. Tully, C. T. Rettner, C. B. Mullins, and D. J. Auerbach, J. Chem. Phys. **94**, 1516 (1991).
[52] R. J. Smith, A. Kara, and S. Holloway, Surf. Sci. **281**, 296 (1993).
[53] R. J. W. E. Lahaye, S. Stolte, S. Holloway, and A. W. Kleyn, Surf. Sci. (in press).
[54] E. F. Greene and E. A. Mason, Surf. Sci. **75**, 549 (1978).
[55] T. C. M. Horn, A. W. Kleyn, and B. Dijkhuis, Chem. Phys. **149**, 275 (1991).
[56] T. C. M. Horn, A. W. Kleyn, and E. A. Gislason, Chem. Phys. **127**, 81 (1988).
[57] E. W. Kuipers, M. G. Tenner, M. E. M. Spruit, and A. W. Kleyn, Surf. Sci. **205**, 241 (1988).
[58] R. J. W. E. Lahaye, S. Stolte, A. W. Kleyn, R. J. Smith, and S. Holloway, Surf. Sci. **307–309**, 187 (1994).
[59] M. J. Weida and D. J. Nesbitt, J. Chem. Phys. **100**, 6372 (1994).
[60] U. Fano and J. H. Macek, Rev. Mod. Phys. **45**, 553 (1973).
[61] C. H. Greene and R. N. Zare, Ann. Rev. Phys. Chem. **33**, 119 (1982).
[62] E. W. Kuipers, M. G. Tenner, S. Stolte, F. H. Geuzebroek, and A. W. Kleyn, Phys. Rev. Lett. **62**, 2152 (1989).
[63] M. G. Tenner, E. W. Kuipers, A. W. Kleyn, and S. Stolte, J. Chem. Phys. **94**, 5197 (1991).